Solid Freeform Fabrication 2019: Proceedings of the 30th Annual International Solid Freeform Fabrication Symposium – An Additive Manufacturing Conference
Reviewed Paper

INKJET PRINTING OF GEOMETRICALLY OPTIMIZED ELECTRODES FOR LITHIUM-ION CELLS: A CONCEPT FOR A HYBRID PROCESS CHAIN

Cara G. Kolb*, Harish R. Mareddy*, Florian J. Guenter*, Michael F. Zaeh*

*Institute for Machine Tools and Industrial Management (*iwb*), Department of Mechanical Engineering, Technical University of Munich, Boltzmannstr. 15, 85748 Garching, Germany

Abstract

Lithium-ion batteries have proven to be reliable energy storage devices for portable and stationary electrical consumers because they possess a high energy and power density. Nevertheless, modern applications require more demanding performance characteristics. Electrodes with a structured surface design, which improves current densities and therefore enables faster charging and discharging, promise to reach the required cell characteristics. Conventionally, structured electrodes are produced by subtractive post-treatment, such as laser processing, which only allows structures of limited complexity. This paper demonstrates a novel approach using inkjet printing to produce electrodes with interlocked structures of high geometrical complexity. A concept for a hybrid process chain that combines the additive process with subtractive and further manufacturing technologies is presented. In addition, a selection of geometrically optimized electrodes is shown. This hybrid process chain has the potential to create functional electrodes by multi-material processing of liquid and powdery raw materials.

Keywords: Inkjet Printing, Lithium-Ion Cell, Multi-Material Processing, Surface Structuring

Introduction and state of the art

The primary goal of most research activities in the field of battery technology is the continuous enhancement of the performance characteristics with a simultaneous improvement of the environmental sustainability and safety. Lithium-ion batteries have a high potential to meet these dedicated goals, as they exhibit a high energy and power density [1]. However, there is still considerable research required regarding the cell components and the cell design to meet the demanding performance requirements of modern applications.

Electrodes with a tailored surface design that reduces the transport distances of the electrons and ions were observed to show positive cell characteristics at high charging and discharging rates [2]. These characteristics are crucial for applications in the electric mobility and mobile end devices as well as for stationary storage devices, which are necessary to cope with high residual loads due to the fluctuating renewable energies in stationary grids. Conventional electrode fabrication processes like slot die coating only allow the generation of flat, unstructured electrode films. Thus, electrode structures can only be produced by subsequent process steps. PROELL ET AL. [3] and HABEDANK ET AL. [4] used laser processing for structuring state-of-the-art electrodes. The studies demonstrated that the fabricated structures were subject to a low complexity. Therefore, in many approaches additive manufacturing (AM) is pursued to fabricate electrode structures with a tailored design in the lower micrometer range. Particular attention has been paid to inkjet printing (IJP), since this technology enables a processing of paste-like raw materials similar to the slurries in the conventional coating process of electrodes [5].

Recent research work includes investigations on the additive manufacturing of supercapacitors [6, 7] and zinc-based batteries [8, 9]. Furthermore, there are first promising feasibility studies for

the layer-by-layer production of anodes [10] and cathodes [11–13] for lithium-ion cells. DELANNOY ET AL. [12] and GU ET AL. [14] fabricated planar, unstructured cathodes on the basis of lithium iron phosphate ($LiFePO_4$, LFP) by using a water-based solvent. Interlocked electrode structures, as already fabricated through Direct Ink Writing, have to the knowledge of the authors not yet been achieved in IJP. In SUN ET AL. [15], the pairing of a lithium titanate ($Li_4Ti_5O_{12}$, LTO) anode with an LFP cathode was investigated. The cell tests showed that the interdigitated electrodes have higher power densities compared to conventionally manufactured, unstructured electrodes.
This paper presents a theoretical concept for using IJP to manufacture three-dimensionally structured electrodes, which are capable of interlocking on a micrometer scale and thus have a high active surface area and shortened lithium ion transport distances. Theoretical approaches are demonstrated that show how the additive process can be integrated into the conventional production chain consisting of subtractive and multiple other technologies. The process steps that are subject to major challenges are dealt with in a separate section.

Hybrid process chain

The development of a hybrid process chain is a prerequisite for industrial manufacturing of printed batteries. For this reason this chapter is meant to propose a new concept of a modified process chain based on the conventional battery production, which incorporates the required sub steps for IJP. The general concept is schematically depicted in Figure 1.

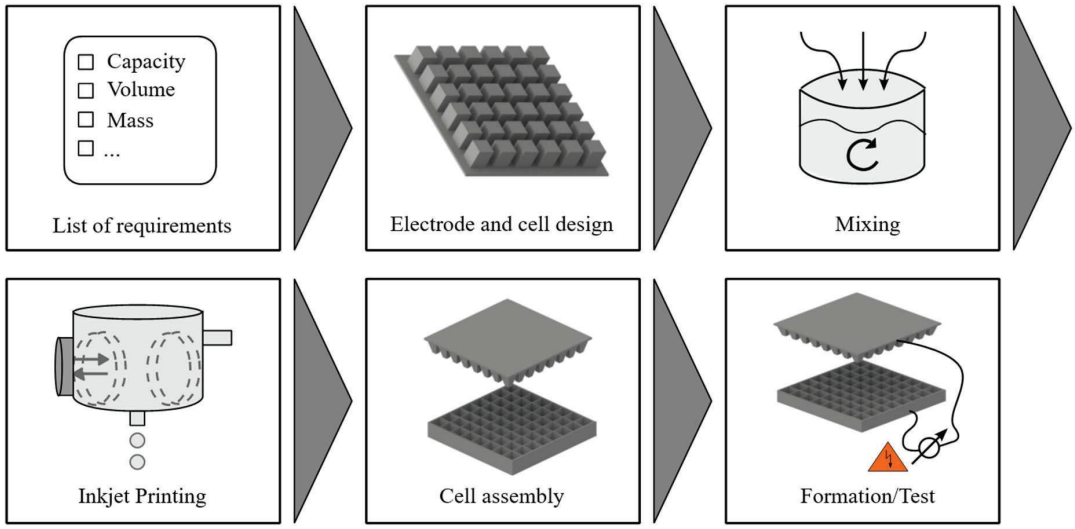

Figure 1: Schematic illustration of the hybrid process chain

The individual sub steps are explained in detail in the following:

List of requirements

Electrochemical storages can be divided into high-energy and high-performance cells. The former are subject to a high specific energy density, but limited in terms of the specific power density. The properties of the latter are the opposite of the high-energy cells and include a

low energy density but achieve a high specific power density. The different performance characteristics are mainly due to the properties of the electrodes. High-energy cells have thick and densely coated electrodes, whereas high-performance cells have thinner and more porous electrodes [16].
Applications for high-energy cells can be found in stationary applications in which no high residuum loads are present. High-performance cells are required for small portable devices for which operation does not require high capacities [17]. With the increasing importance of batteries for applications that combine the characteristics of both cell designs (e.g. electric mobility), power sources with a high areal capacity Q (mAh/mm^2) and high discharge power capabilities are increasingly needed [18]. An electrode structuring using additive manufacturing can achieve this. Additionally, there are specific requirements for safety, lifetime and environmental sustainability depending on the application area.
This shows the variety of requirements that can be posed to electrical storage devices. In order to address the application-specific requirements during the design and the production of the battery, its future properties must be initially clarified and systematically summarized, e.g. in a list of requirements.

Electrode and cell design

Based on the list of requirements, the customized electrode and thus the cell design is determined. Approaches for the identification of optimized electrode structures are shown in Section “Identification of geometrically optimized electrode structures”.
Additionally, suitable materials are selected for the anode and the cathode depending on the application and the respective demands. High safety requirements limit the amount of suitable materials, as a large number of potential materials such as the cathode material lithium nickel manganese cobalt oxide (LiNiMnCoO, NMC) have a significant hazard potential [19].
Subsequently, the data models of the desired electrode geometries are generated in a CAD program. The required allowance to compensate for the shrinkage induced by the drying process is calculated in advance and taken into account in the digital data model. The estimation of the dry layer is a challenging task. The evaporation of the solvent is assumed to lead both to a slight reduction in the layer thickness and also to an increase in the porosity of the manufactured electrodes.
In the following, the standard triangulation language (STL) model is divided into slices. The minimum wet film thickness primarily depends on the nozzle diameter and distance as well as on the characteristics of the processed slurry and lies usually in the range between $50\,nm$ and $100\,\mu m$ [20].
Finally, the electrode structures to be manufactured are digitally positioned and oriented on the building platform in the assembly space and a suitable set of process parameters is defined. While most commercially available printer systems only support the setting of elementary process parameters such as the print speed, all parameters for controlling the respective subsystems should be adjustable in a system tailored for IJP of electrodes. Consequently, the process parameters can be individually adapted to the respective materials. This includes, for example, the input voltage signal of the piezoelectric sensor which triggers the drop formation, the feed rate, the print and the travel speed, the distance between the print head and the platform as well as the temperature of the printer head induced by a coupled heating unit.

Mixing

The purpose of mixing is to produce a homogeneous slurry consisting of the active material, binder, additives and solvent which can be processed in IJP.
Conventionally, mixing includes two main processes: dry and wet mixing (see Figure 2).

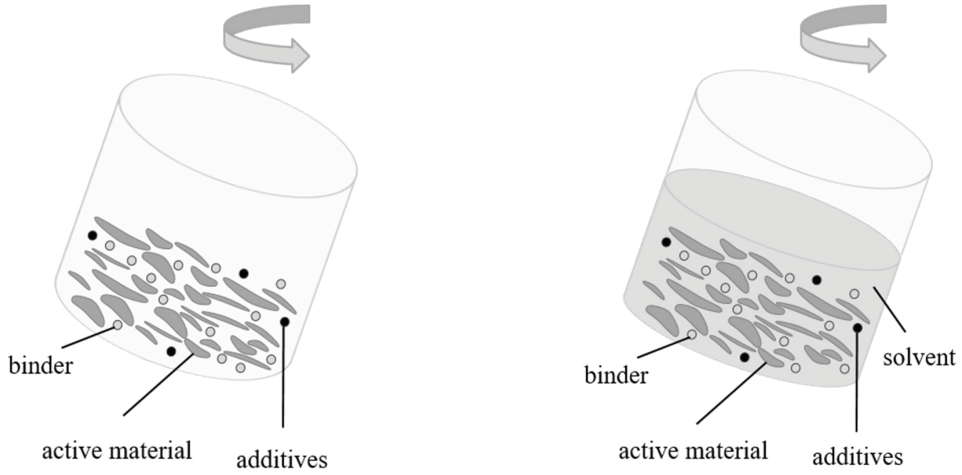

(a) (b)

Figure 2: Schematic depiction of the principle of (a) dry mixing and (b) wet mixing

The former describes the blended mixing of active materials with binder and conducting additives (where appropriate), which are all available in powder form. The binder is used for good cohesion between the particles within an electrode and also a sufficient adhesion to the respective current collectors [21]. Wet mixing describes the part of the process in which solvent is added successively to the mixture. N-methylpyrrolidone (NMP) in the combination with the binder polyvinylidene fluoride (PVDF) is most commonly used as a solvent [22]. Due to the distinct volatility and the potentially harmful effect to pipes and components in the print head, suspensions on the basis of this chemical compound are considered hardly suitable for IJP. A less aggressive and environmentally friendly alternative is water, but this also requires the use of water-based binder materials such as carboxymethyl cellulose (CMC) or styrene-butadiene rubber (SBR) [23, 24]. However, some cathode materials such as high-energy NMC (HE-NMC) are sensitive to water and require different solvents for printing [25]. This exhibits that the potentially suitable solvents have advantages and disadvantages and must be selected depending on the respective anode and cathode materials. Nevertheless, water is assumed to represent a suitable solvent for the majority of relevant active materials. Previous works have already demonstrated the applicability of water as a solvent for graphite [26], graphene [27], LTO [15] and LFP [12, 14–15].
Additionally, additives may be required to prevent the formation of agglomerates as well as to stabilize the slurry in order to inhibit sedimentation (see Figure 3) [20].
For a stable and reliable processing of the suspension within a print head, the particle size of the input materials should not exceed $1/50$ of the nozzle diameter [28]. UTELA ET AL. [29] even reported a threshold value of $1/100$. A print head can contain up to several hundred nozzles. Depending on the nozzle diameter and the distance, a resolution of 100 to 5000 dpi is achieved with a wet film thickness ranging from 50 nm to 100 µm [20]. However, there is a conflict of

objectives between the nozzle diameter and the attainable resolution of the printed structures. The larger the nozzle diameter, the smaller is the resolution.
Since the particle size distribution of electrochemical powders is also in the lower micrometer range [30, 31], processing without any adaptions of the powder, the print head or both is not possible. Furthermore, the suspension characteristics have to be adapted to the printing process to ensure the formation of stable droplets (see Figure 3). As this requires a lot of research in advance, an approach for adjusting the electrochemical suspension on the print head and vice versa is presented in Section "Approach for the reliable processing of an electrochemical suspension in IJP."

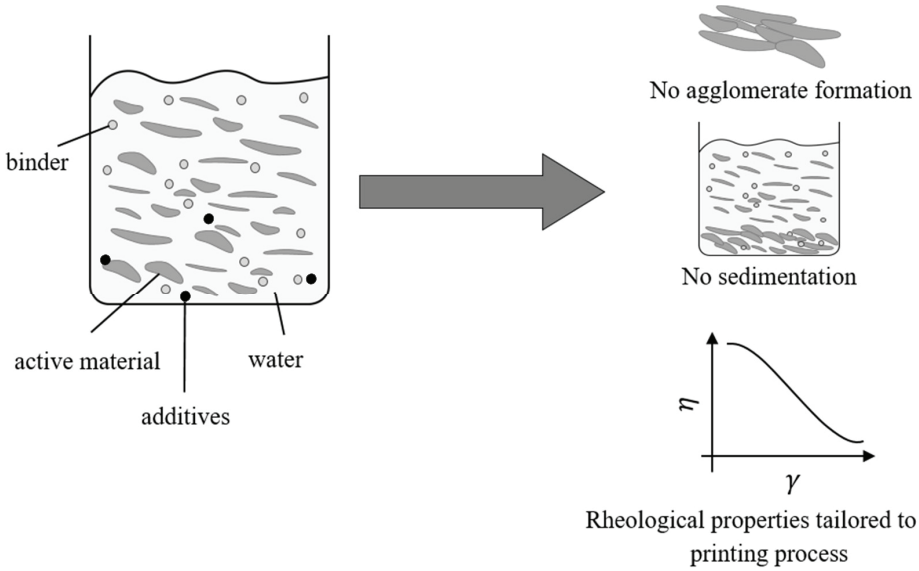

Figure 3: Characteristics of a printable suspension in IJP (η: dynamic viscosity, γ: shear rate)

Inkjet printing

This step is divided into three subprocesses; *pre-processing*, *processing* and *post-processing*. The process chain described in the following represents a concept in which the cathode and anode structures are fabricated in separate manufacturing processes.

Pre-Processing

Initially, the current collectors, which consist of thin metal foils, may undergo a plasma treatment to roughen the surface and thereby contribute to a more enhanced adhesion of the deposited suspension [32]. Commonly, copper is utilized for the anode and aluminum for the cathode. The thickness of the aluminum foil can be found in the range between 10 to 20 µm [32], whereas the copper foil is in the range between 4 and 12 µm [33].
The respective current collector has to be attached to the building platform in a fixed position. Due to the low thickness, it is expected that this will be a major challenge. It is conceivable that a vacuum adapter plate is installed on top of the building platform for this purpose [34]. Similar problems can be found for positioning thin probes in a microscope or profilometer.

Processing

The actual printing process is characterized by the layerwise fabrication of the electrode on the basis of the digital data set. The process steps – *application of a new layer*, *solidification of the layer (evaporation of solvent)* and *elevating of the print head* or *lowering of the building platform* – are repeated iteratively until the complete electrode structure is formed (see Figure 4).

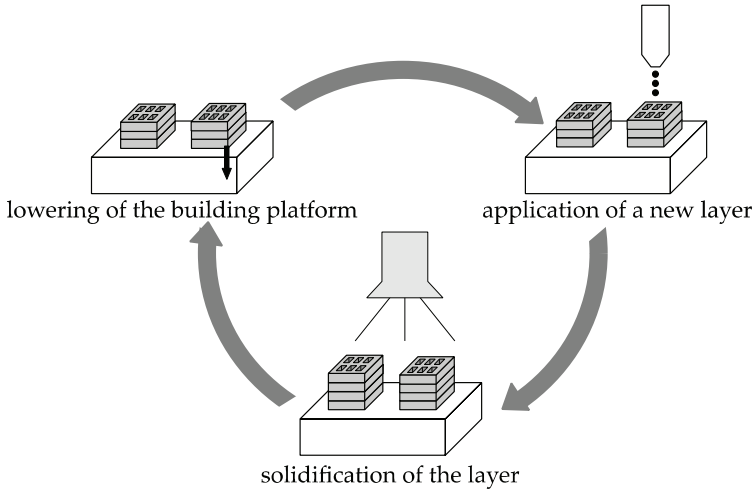

Figure 4: Schematic illustration of the process with the respective process steps

In contrast to the conventional production chain, the IJP process enables the targeted deposition of the suspension on the current collector directly where the later electrode is created. This leads to an efficient use of the costly raw material powder. In order to prevent a blurring of the individual layers and thus to enable a high degree of shape retention, layerwise drying is required. The degree of drying must be carried out in such a way that good adhesion of the respectively subsequent layer is guaranteed. The drying method should be adapted to the absorption behavior of the used solvent. Water, for example, primarily absorbs medium wave radiation and then converts it directly into heat, leading to a particularly quick evaporation. Therefore, infrared lamps that are characterized by medium wave radiation are suitable for drying water-based suspensions [35]. Additionally, during processing the formation of capillary forces in the fine channels of the print head must be avoided, since this causes the remaining nanoparticles to accumulate on the walls and clog the channels. Consequently, the print head, including the nozzles, remains completely flooded, reducing the free surfaces between the fluid and the atmosphere to a minimum.

In order to guarantee a stable printing process, after which the fabricated electrodes meet the quality requirements, a comprehensive process monitoring or controlling concept respectively is needed. Rudimentary approaches for this can be found in the literature:

In [36], a concept for monitoring the droplet formation at the print head employing ultrasound is described. During the generation of drops, pressure fluctuations occur near the nozzle due to the highly dynamic emission of the suspension, which can be measured with a suitable acoustic sensor. An absent signal or deviations from the expected signature indicate a problem in the respective nozzle. Furthermore, an approach of optically analyzing the substrate by means of a camera to detect defective nozzles during the printing process was recently demonstrated [37].

Both approaches are suitable for print head variants, in which the nozzles are arranged such that several nozzles can reach a certain point on the substrate, depending on the kinematics of the printer. Consequently, a control mechanism can be implemented directly into the printer's firmware by sequentially controlling the nozzles and analyzing the resulting acoustic signals. If deviations are detected, the system attempts to identify and deactivate the respective nozzle as well as compensate for the defective nozzle by using another remaining nozzle.

Post-Processing

The manufactured electrodes are separated from the platform. For this purpose, the vacuum is degraded. Subsequently, the building platform is cleaned with isopropanol in order to avoid a contamination of the current collector foils. Furthermore, residues of the suspension in the print head, including all channels and nozzles, must be removed using a suitable cleaning agent. The manufactured electrodes are treated in a drying process with a vacuum furnace to remove the residual humidity, which is indispensable for the subsequent cell assembly.

Cell assembly

The cell assembly is conducted in a dry room at an ambient temperature of $22° C \pm 2° C$ with a dew point of $-42° C$, equivalent to a relative humidity of < 1 % [38]. The porosity of the fabricated electrodes, which is a function of the electrode thickness, is calculated. Due to the three-dimensional structures, the thickness is not constant over the length, width or diameter of the electrode. To overcome this issue, an average electrode thickness is assumed. As a result, the porosity can only be approximated. Based on this, it has to be evaluated whether a calendaring process is required. The aim is to achieve the desired porosity only by well-set process parameters. For example, it is expected that the porosity can be adjusted selectively by the targeted activation or deactivation of adjacent nozzles.

Subsequently, the current collectors and separators are customized with regard to the required format of the cell. Due to the targeted deposition of the slurry, the active material does not have to be cut to size. Currently, the electrode cutting process is realized by die cutting or laser cutting. The latter provides a high flexibility of the cutting pattern, which may be of major importance for the individual structures enabled by IJP. In the subsequent cell formation, the anode-separator-cathode pairs are oppositely arranged and fixed. Current collectors coated only on one side can be generated with the process chain described in this paper. Fabricating current collectors coated on both sides in order to increase the energy density requires further modifications in the IJP machine. They are welded together to obtain an electrical and mechanical connection between the current collectors of the positive and negative electrode. This process step is followed by packaging the cell stack. Steel and aluminum are often utilized as casing materials. The housing both prevents the entrance of humidity and dust into the cell and enables the uptake of electrolyte in the subsequent filling and wetting process. This process is technologically sophisticated and marks a decisive progress towards the functionality of the cell. Previous studies have even demonstrated that laser structured electrodes were subject to a significant reduction of the time required for a complete wetting [39]. This emphasizes that the structuring of the electrodes has the potential to contribute to an accelerated lead time. Commonly, an electrolyte for lithium-ion batteries is in a liquid state and consists of a combination of conductive salts, an organic aprotic solvent and additives. Furthermore, polymer electrolytes are used, which in the current design assume both the role of the separator and the electrolyte [40, 41]. It is expected that the latter type of electrolyte is printable in IJP, as it is in a gel-like condition. Finally, the packaging is sealed.

Formation/Quality assurance

The formation refers to the first charging and discharging cycles of the cell under defined conditions. Within this process a passivation layer, the so-called solid electrolyte interface (SEI), is formed at the interface between the active material of the anode and the electrolyte due to the decomposition of the electrolyte [42]. To the knowledge of the authors, the influence of the electrode structure on the formation of the SEI has not been investigated so far. This is intended to be done by postmortem investigations in which the cyclized cells are reopened and various analyses are carried out. For quality assurance purposes, cell tests are conducted. A major challenge during this is the comparability of electrodes with different structures, since the areal capacities fluctuate over the diameter of the electrode. This implies that a straightforward comparison of the absolute capacity retention is not possible.

Identification of geometrically optimized electrode structures

The primary goal of electrode structuring is the active shortening of the ion paths as well as the simultaneous increase of the surface-area-to-volume ratio [43, 44]. This is expected to lead to a reduced internal resistance of the cell and thus to an enhanced charge and discharge capability [2].

In a preliminary study, exemplary electrode designs with the same loading were designed in a CAD program and meshed (see Figure 5). The counter electrode represents the negative part of the interlocking design, but is, for purposes of clarity, not shown. Table 1 shows the specifications of the base electrode.

Table 1: Specifications of the investigated base electrode

Specific feature	Value
Dimensions of the base of the electrode	$2\ mm\ x\ 2\ mm$
Base area of the electrode	$4\ mm^2$
Volume of material	$0.5\ mm^3$

The Hilbert base extrude was inspired by the internal structures of fern leaves, which are known for their efficient platform for energy storage in biological processes. The internal structures were reconstructed by using the mathematical Hilbert fractal curve [45].

For an initial assessment, the surface area was determined. Furthermore, the mean ion and electron transport distance were calculated by means of the k-nearest neighbors' (k-NN) algorithm (see Figure 5) which is widely used as a classification algorithm in Machine Learning [46]. K-NN represents a classification method in which a class is assigned taking into account its k closest neighbours. The principle of k-NN is schematically depicted in Figure 6. Figure 6a shows two sets of data points, one in blue and the other in green. Among these, an unknown point (marked in red) needs to be classified as either blue or green. Hence, the whole space is tessellated into Polygonal regions called Voronoi cells (see Figure 6b). A polygon region is constructed around each point in which all points in that region are only closer to that corresponding point than to any other point. The unknown point (marked in red) thus falls into the Voronoi cell of a green point and is therefore classified as green.

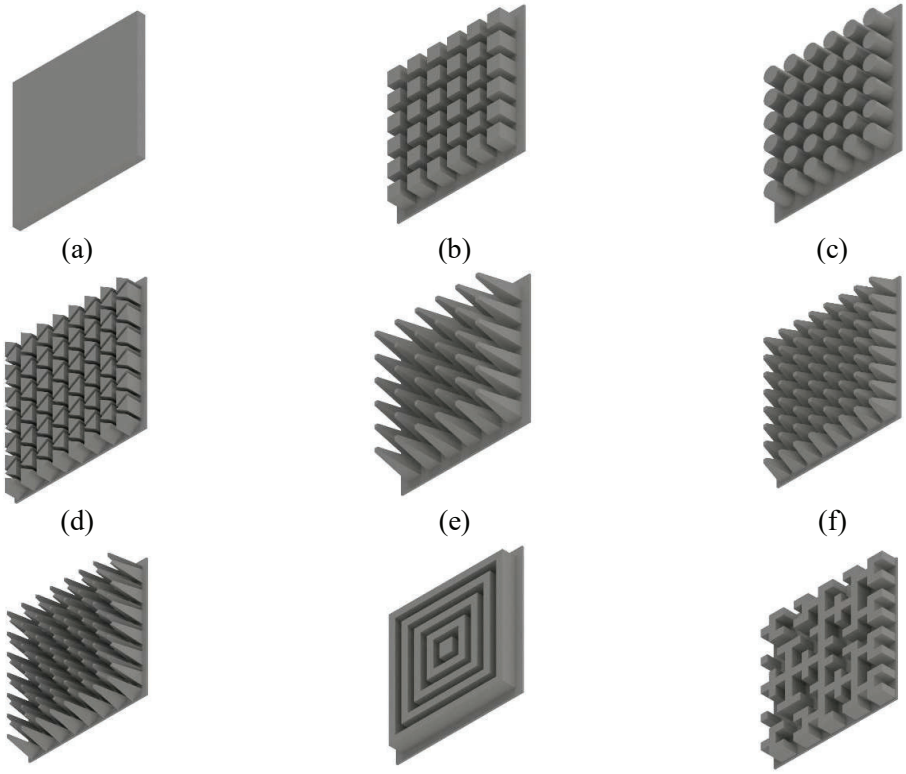

Figure 5: Selection of investigated electrode structures: (a) unstructured electrode, (b) square base extrude, (c) cylinder extrude, (d) triangle base extrude, (e) square base pyramid 6x6, (f) square base pyramid 8x8, (g) triangle base pyramid, (h) concentric square, (i) Hilbert fractal base extrude

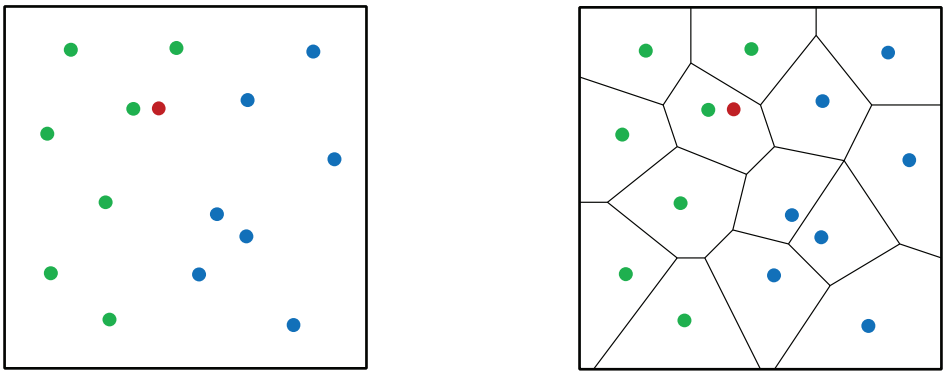

Figure 6: Schematic depiction of the Voronoi cells in k-NN search with the data set A (marked in green), the data set B (marked in blue) and the unknown point (marked in red) (modified from [46])

From Figure 7, the following conclusions can be drawn:

- The structured electrodes have a higher surface area than the flat electrode.
- Irrespective of the shape of the base (square/triangle), the pyramidal structures show lower mean ion transport distances compared to non-pyramidal structures.
- Pyramidal structures have a higher surface area than non-pyramidal structures. In particular, the triangle base electrodes have a higher surface area than the square base and the cylindrical electrodes.
- All electrode designs have a higher mean electron transport distance than the flat electrode. However, it was reported that the rate performance is mainly limited by the electrolytic conductivity and the Li^+ diffusivity and not by the electronic conductivity, especially at high current rates [43, 44].

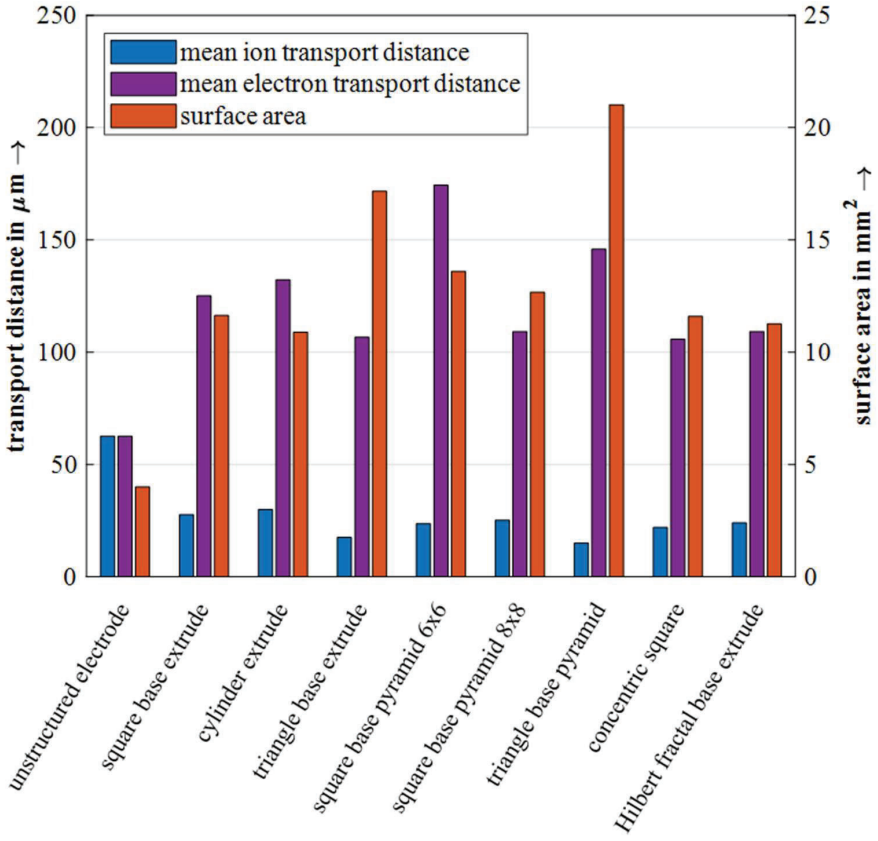

Figure 7: Mean transport distances for ion and electron charge and surface area for different electrode designs

The aim of future work must be to examine whether the simulation approach from [45] can be transferred to interlocking structures. The goal is to develop an electrochemical model, which describes the relationship between the geometric dependencies and the electrical characteristics (e.g. rate capability) directly. Consequently, the capacity progression during the charging and discharging cycles could be predicted.

Approach for the reliable processing of an electrochemical suspension in IJP

Previously, it was demonstrated that a wet grinding of commercially available powder in a planetary micro mill prior to the mixing process leads to a reduction of the entirety of raw particles below the limit value for printing [10]. Subsequently, the aqueous mixture was further diluted and mixed in a commercially available mixer. Other authors processed electrochemical suspensions based on commercially available nanopowders whose particle sizes were already below the threshold [12]. Therefore, a novel approach is suggested here, since the grinding process is assumed to lead to a destruction of the atomic structure of especially complex composite structures optimized for the application in a lithium-ion cell. As a result, the modified material may be restricted in the capability of intercalating ions. Furthermore, it is expected that the effect of lithium plating is more significant due to the higher entire particle surface, which leads to a reduced total capacity. This mechanism consists of the formation of a metallic lithium phase on the surface of the anode during charging [50]. The introduced concept aims at a reliable processing of the respective electrochemical suspensions by either isolating the particles with additives or by a modification of the print head system. In addition, a procedure is shown for creating a suspension whose characteristics are adequate for the developed print head system. The authors have recently started working on the following items.

Modification of the suspensions by means of rate performance tests

Clogging due to particle fractions with high diameters and agglomeration can be prevented by adding shear thickening substances such as xanthan [51] or methylcellulose [52] to the mixture. Furthermore, the addition of a secondary fluid leading to a high viscosity at low shear stress such as 1-octanol [53] is conceivable. This leads to an encapsulation of the single particles in the condition of rest situation as it appears in the print head or the reservoir. It is expected that significantly larger particle fractions can still be processed without leading to clogging. However, this is only feasible if the additives have no significant influence on the electrochemical properties of the final electrode. This can be examined by conducting rate performance tests of half cells (lithium foil as counter electrode) based on planar electrodes fabricated from the produced suspensions.

Modifying the print head by means of a morphological box and potential analysis

If modifying the suspensions is not feasible for a reliable printing of the electrochemical suspensions, measures have to be implemented at the print head. The aim of these measures is to extract particles beyond the threshold value (see Section “Mixing” in Section “Hybrid process chain”) which is in the order of a few µm for commercially available print head systems. Suitable measures are identified on the basis of a morphological box and selected by means of a methodical potential analysis. Subsequently, the suitability is examined in ex-situ studies.

Identifying printable suspensions by means of a physical analysis based on experiments

The properties of the respective electrochemical suspensions have to be adjusted to the nozzle geometry of the emerging prototype in order to ensure stable droplet formation and thus excellent printing quality. ZHANG ET AL. [5] proposed to use the Ohnesorge number Oh for electrochemical suspensions to predict whether the formation of a stable droplet can be expected. Since the Ohnesorge number is only valid for Newtonian fluids [54, 55] and most electrochemical suspensions show a shear thinning behavior due to the high solid content [12, 56], the following approach in parts based on DELANOY ET AL. [12] is pursued.

The diameter of the smallest feasible ejecting orifice is determined by screening the particle size distribution of relevant starting materials with regard to the fractions above the threshold range (see Subsection "Mixing" in Section "Hybrid process chain"). This is additionally influenced by the suitability of additives or respectively the effectiveness of the identified measures at the print head (see previous sections). If the former approach is not suitable for the application, the tendency of the particles to format agglomerates has to be accounted for as well. This is assessed by means of zeta potential [57] and Stokes radius measurements [58].
Subsequently, the stability of the suspensions at rest condition (storage in the print head) is examined. Therefore, the storage modulus (G') (elastic portion of the complex modulus G^*) and the loss modulus (G'') (viscous portion of G^*) are measured over time at constant strain and frequency. The phase shift δ describes the ratio of the elastic and viscous proportion. If δ is between 0 and $45\,°$, the characteristics of a solid predominate and sedimentation as well as agglomeration are inhibited [59]. On this basis, the solid content, the proportion of dispersants and the ratio of shear thickening additives are systematically varied (input variables) and the resulting course of δ is evaluated.
With the calculated radius of the ejecting orifice r (usually in the range of the droplet radius) and the targeted volume flux Q, the wall shear rate, as it applies for nozzle-based processes, is determined as follows [60]:

$$\dot{\gamma}_{wall} = \frac{4Q}{\pi r^3} \tag{1}$$

This is followed by investigations on the dynamic viscosity η (see Figure 5) and the imposed shear stress σ. The former is dependent on the temperature T, the pressure p, the time span t and the shear rate $\dot{\gamma}$. A multiple regression analysis based on the limitations resulting from the investigations at rest situation is performed. The target properties of a shear thinning suspension suitable for printing can be defined as follows [12] (see Figure 8):

- High viscosity at rest conditions (storage in the print head)
- Low viscosity at high shear rate (shearing of droplets)

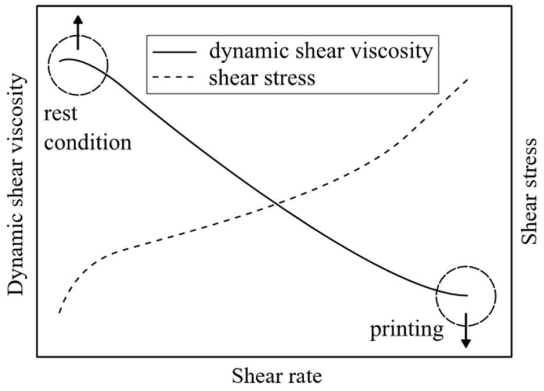

Figure 8: Schematic illustration of the curves of the dynamic shear viscosity η and the shear stress σ as a function of the shear rate γ; the regimes for rest conditions (print head) and the printing process are highlighted. (modified from [20])

After printing, the electrochemical suspensions must be adjusted to achieve rapid and continuous reforming of the rest conditions [12]. Otherwise, the droplets would expand and thus lead to a blurring of the printing pattern.

Design of a prototypical print head

A prototypical print head enabling a free adjustment of all-important process parameters (e.g. voltage signal and temperature) is implemented. An additional heating element is integrated that allows a further fine adjustment of the dynamic viscosity. The nozzle geometry is based on commercially available systems in order to ensure a transferability to other systems in the context of later upscaling. Within this prototype, the previously identified measures are implemented, and their feasibility is evaluated. With the aim of a high reproducibility of the droplet formation and thus a constant shear rate, a volume-controlled operation of the piezoelectric sensor is applied. For this purpose, the volumetric flow is measured continuously at the nozzles and the voltage is regulated on this basis. The process of the droplet formation, separation and regression on the current collector foil is observed by a high-speed camera, whereby a process laser is used to illuminate the area close to the print head or respectively the building platform.

Conclusion and Outlook

An approach was demonstrated showing how to qualify IJP for fabricating geometrically complex electrodes with interlocked structures on laboratory scale. A concept of an adapted hybrid process chain linking the IJP process with the required process steps for the battery production was presented. In this context, the individual substeps were analyzed with regard to their suitability for IJP of electrochemical slurries and conceivable modifications were specified where necessary. Furthermore, an approach for the reliable processing of an electrochemical suspension in IJP was presented. With this procedure, the properties of suspensions can be adjusted to the characteristics of the nozzle by analytical and experimental studies. Hence, the results of this manuscript can contribute to the transfer from laboratory to industrial scale for fabricating large-format cells based on structured electrodes. Furthermore, the findings can also be transferred to relevant materials for solid state batteries. Due to the inherent ability to process multiple materials by installing additional printer head units for any further suspension, IJP offers good conditions for the layer-by-layer fabrication of an entire solid-state battery cell in a single manufacturing process.

Acknowledgments

This research did not receive any specific grant from funding agencies in the public or commercial sectors. The authors extend their sincere gratitude to the *iwb e.V.* for tits faith in this research topic and for supporting further investigations within this field.

References

[1] Scrosati, B; Garche, J., Journal of Power Sources 195 (2010) 9, pp. 2419–2430.

[2] Habedank, J.B.; Kraft, L.; Rheinfeld, A.; Krezdorn, C.; Jossen, A.; Zaeh, M.F., Journal of The Electrochemical Society 165 (2018), pp. 1563–1573, 10.1149/2.1181807jes.

[3] Proell, J.; Kim, H.; Piqué, A.; Seifert, H.J.; Pfleging, W., Journal of Power Sources 255 (2014), p. 116–124, 10.1016/j.jpowsour.2013.12.132.

[4] Habedank, J.B.; Endres, J.; Schmitz, P.; Huber, H.P.; Zaeh, M.F., Journal of Laser Applications 30 (2018), p. 032205, 10.2351/1.5040611.
[5] Zhang, F.; Wei, M.; Viswanathan, V.V.; Swart, B.; Shao, Y.; Wu, G.; Zhou, C., Nano Energy 40 (2017), pp.418–431, 10.1016/j.nanoen.2017.08.037.
[6] Choi, K.-H.; Yoo, J.; Lee, C. K.; Lee, S.-Y., Energy & Environmental Science 9 (2016), pp. 2812–2821, 10.1039/C6EE00966B.
[7] Le, L. T.; Ervin, M. H.; Qiu, H.; Fuchs, B. E.; Lee, W. Y., Electrochemistry communications 13 (2011) , pp. 355–358, 10.1016/j.elecom.2011.01.023.
[8] Ho, C. C.; Murata, K.; Steingart, D. A.; Evans, J. W.; Wright, P. K., Journal of Micromechanics and Microengineering 19 (2009), pp. 94013, 10.1088/0960-1317/19/9/094013.
[9] Hilder, M.; Winther-Jensen, B.; Clark, N. B., Journal of Power Sources 194 (2009), pp. 1135–1141, 10.1016/j.jpowsour.
[10] Zhao, Y.; Zhou, Q.; Liu, L.; Xu, J.; Yan, M.; Jiang, Z., Electrochimica Acta 51 (2006), pp. 2639–2645, 10.1016/j.electacta.2005.07.050.
[11] Huang, J.; Yang, J.; Li, W.; Cai, W.; Jiang, W., Thin Solid Films 516 (2008), pp. 3314–3319.
[12] Delannoy, P.-E.; Riou, B.; Brousse, T.; Bideau, J. L.; Guyomard, D.; Lestriez, B., Journal of Power Sources 287 (2015), pp. 261–268, 10.1016/j.jpowsour.2015.04.067.
[13] Milroy, C. A.; Jang, S.; Fujimori, T.; Dodabalapur, A.; Manthiram, A., Small 13 (2017), pp. 1603786, 10.1002/smll.201603786.
[14] Gu, Y.; Wu, A.; Sohn, H., Nicoletti, C.; Iqbal, Z.; Federici, J. F., Journal of Manufacturing Processes 20 (2015), pp. 198–205, 10.1360/972013-794.
[15] Sun, K.; Wei, T. S.; Ahn, B. Y.; Seo, J. Y.; Dillon, S. J.; Lewis, J. A., Advanced materials 25 (2013), pp. 4539–4543, 10.1002/adma.201301036.
[16] Singh, M.; Kaiser, J.; Hahn, H., Journal of the Electrochemical Society 162 (2015), pp. A1196-A1201, 10.1149/2.0401507jes.
[17] Bates, J.B.; Dudney, N.J.; Neudecker, B.; Ueda, A.; Evans, C.D., Solid State Ionics 135 (2000) 1-4, pp. 33–45, 10.1016/S0167-2738(00)00327-1.
[18] Kang, K.; Meng, Y.S.; Bréger, J.; Grey, C.P.; Ceder, G., Science 311 (2006) 5763, pp. 977–980, 10.1126/science.1122152.
[19] Sun, J.; Li, J.; Zhou, T.; Yang, K.; Wei, S.; Tang, N.; Dang, N.; Li, H.; Qiu, X.; Chen, L., Nano Energy 27 (2016), pp. 313–319, 10.1016/j.nanoen.2016.06.031.
[20] Lanceros-Méndez, S.; Costa, C.M., John Wiley & Sons. ISBN: 978-1-119-28742-1.
[21] Billot, N.; Guenther, T.; Schreiner, D.; Stahl, R.; Kranner, J.; Beyer, M.; Reinhart, G., Energy Technology (2019),10.1002/ente.201801136.
[22] Wood III, D.L.; Li, J.; Daniel, C., Journal of Power Sources 275 (2015), pp. 234–242, 10.1016/j.jpowsour.2014.11.019.
[23] Marchini, M.; Nobili, F.; Tossici, R.; Wohlfahrt-Mehrens, M.; Marassi, R., Journal of Power Sources 196 (2011), pp. 9665–9671, 10.1016/j.jpowsour.2011.07.028.

[24] Zhang, R.; Yang, X.; Zhang, D.; Qiu, H.; Fu, Q.; Na, H.; Guo, Z.; Du, F.; Chen, G.; Wie, Y., Journal of Power Sources 285 (2015), pp. 227–234, 10.1016/j.jpowsour.2015.03.100.
[25] Jung, R.; Morasch, R.; Karayaylali, P.; Philips, K.; Maglia, F.; Stinner, C.; Shao-Horn, Y.; Gasteiger, H.A., Journal of the Electrochemical Society 165 (2018), pp. A132–A141, 10.1149/2.0401802jes.
[26] Lis, M.; Chudzik, K.; Bakierska, M.; Świętosławski, M.; Gajewska, M.; Rutkowska, M.; Molenda, M., Journal of The Electrochemical Society, 166 (20119), pp. A5354-A5361.
[27] Liu, W.R.; Kuo, S.L.; Lin, C.Y.; Chiu, Y.C.; Su, C.Y.; Wu, H.C.; Hsieh, C.T.; The Open Materials Science Journal, *5* (2011), pp.236-241.
[28] Hutchings, I.M.; Martin, G.D., John Wiley & Sons (2012). ISBN: 978-0-470-68198-5.
[29] Utela, B.; Storti, D.; Anderson, R.; Ganter, M., Journal of Manufacturing Processes 10 (2008), pp. 96–104, 10.1016/j.jmapro.2009.03.002.
[30] Sigma-Aldrich: Product Specification: Lithium Nickel Manganese Cobalt Oxide. < https://www.sigmaaldrich.com/catalog/product/aldrich/761001?lang=de&region=DE>
[31] Sigma-Aldrich: Product Specification: Graphite. <https://www.sigmaaldrich.com/Graphics/COfAInfo/SigmaSAPQM/SPEC/28/282863/282863-BULK_____ALDRICH__.pdf>
[32] Nakanishi, S.; Suzuki, T.; Qi, C.U.I.; Akikusa, J.; Nakamura, K., Transactions of Nonferous Metals Society of China 24 (2014), pp. 2314–2319.
[33] Targray: Electrodeposited Copper Foils (2018) <https://www.targray.com/li-ion-battery/foils/copper>
[34] Ozawa, K., US Patent 5,542, 726.
[35] Kajtna, J.; Šebenik, U.; Krajnc, M.; Golob, J., Drying Technology 26 (2008), pp. 323–333, 10.1080/07373930801898059.
[36] Su, W.L.; Benjamin, T.L.; Elgee, S.B.; Uhling, T.F.; Axten, B.A.; Lundsten, K.J.; Man, X.C.; Hahn, T.L.; Dangelo, M.T.; Woll, B.D.; Weber, T.L., US Patent 6 260 941.
[37] Childers, W.D.; Askeland, R.A.; Li, G., US Patent 7,607, 752.
[38] Reinhart, G.; Zeilinger, T.; Kurfer, J.; Westermeier, M.; Thiemann, C.; Glonegger, M.; Wunderer, M.; Tammer, C.; Schweier, M.; Heinz, M., Future Trens in Production Engineering (2013), pp. 3–12, 10.1007/978-3-642-24491-9_1.
[39] Habedank, J.B.; Guenter, F.J.; Billot, N.; Gilles, R.; Neuwirth, T.; Reinhart, G.; Zaeh, M.F., The International Journal of Advanced Manufacturing Technology (2019), pp. 1–10., 10.1007/s00170-019-03347-4.
[40] Meyer, W.H., Advanced Materials 10 (1998), pp. 439–448, 10.1007/s11581-016-1908-6.
[41] Zhang, S.S., Journal of Power Sources 164 (2007), pp. 351–364, 10.1016/j.jpwsour.2006.10.065.
[42] Verma, P.; Maire, P.; Novák, P., Electrochimica Acta 55 (2010), pp. 6332–6341, 10.1016/j.electacta.2010.05.072.
[43] Long, J.W.; Dunn, B.; Rolison, D.R.; White, H.S., Chemical Reviews 104 (2004), pp. 4463–4492, 10.1021/cr020740I.

[44] Ebner, M.; Chung, D.-W.; García, R.E.; Wood, V., Advanced Energy Materials 4 (2014), p. 1301278, 10.1002/aenm.201470024.
[45] Thekkekara, L.V.; Gu, M., Scientific reports 7 (2017), p. 45585, 10.1038/srep45585.
[46] Okabe, A., Boots, B., Sugihara, K. and Chiu, S.N., John Wiley & Sons, 2009.
[47] Byles, B.W.; Palapati, N.K.R.; Subramanian, A.; Pomerantseva, E., APL Materials 4 (2016), p. 046108, 10.1063/1.4948272.
[48] Assano, T.; Yubuchi, S.; Sakuda, A.; Hayashi, A.; Tatsumisago, M., Journal of the Electrochemical Society 164 (2017), pp. A3960–A3963, 10.1149/2.1501714jes.
[49] Newman, J.; Thomas-Alyea, K.E., John Wiley & Sons, 2014. ISBN: 978-0471477563.
[50] Petzl, M.; Kasper, M.; Danzer, M.A., Journal of Power Sources 275 (2015), pp. 799–807, 10.1016/j.jpowsour.2014.11.065.
[51] He, J.; Zhong, H.; Wang, J.; Zhang, L., Journal of alloys and compounds 714 (2017), pp. 409–418, 10.1016/j.jallcom.2017.04.238.
[52] Amboon, W.; Tulyathan, V.; Tattiyakul, J., Food and bioprocess technology 5 (2012), pp. 601–608, 10.1007/s11947-010-0327-3.
[53] Alamán, J.; Alicante, R.; Peña, J.; Sánchez-Somolinos, C., Materials 9 (2016), p. 910, 10.3390/ma9110910.
[54] Bitsch, B., Dittmann, J., Schmitt, M., Scharfer, P., Schabel, W.; Willenbacher, N.; Journal of Power Sources, 265 (2014), pp.81-90.
[55] Clasen, C.; Phillips, P.M.; Palangetic, L.; Vermant, A.J., AIChE Journal 58 (2012) 10, pp. 3242–3255, 10.1002/aic.13704.
[56] Guenther, T.; Billot, N.; Schuster, J.; Schnell, J.; Spingler, F.B.; Gasteiger, H.A., Advanced Materials Research 1140 (2016), pp. 304–311. Trans Tech Publications, 10.4028/www.scientific.net/AMR.1140.304.
[57] Tsai, F.Y.; Jhang, J.H.; Hsieh, H.W.; Li, C.C., Journal of Power Sources 310 (2016), pp. 47–53, 10.1016/j.jpowsour.2016.02.003.
[58] Bauer, W.; Noetzel, D., Ceramics International 40 (2014), pp. 4591–4598, 10.1016/j.ceramint.2013.08.137.
[59] Porcher, W.; Lestriez, B.; Jouanneau, S.; Guyomard, D., The Journal of the Electrochemical Society 156 (2009), pp. A133–A144, 10.1149/1.3046129.
[60] Darby, R., Darby, R. and Chhabra, R.P., CRC Press (2001).